[PROC. OF JSCE Structural Eng. /Earthquake Eng. Vol. 2, No. 1 April 1985]

WIND TUNNEL STUDY ON GALLOPING OSCILLATIONS OF SUSPENDED FIGURE-8 TELECOMMUNICATION CABLES

*Manabu ITO**, *Yozo FUJINO*** *and Hiroki YAMAGUCHI****

It has been reported that many telecommunication cables of figure-8 section suffered from operating problems and sometimes even failed because of wind-induced large amplitude oscillation, the so-called galloping of cable. In this study, three-dimensional figure-8 cable models are tested at the wind tunnel and aeroelastic behaviour of the cable was observed in detail. It is found that wind-induced significant change of the angle of attack of the cable relative to wind is the fundamental cause of galloping. The critical wind speed that triggered galloping and the initial direction of the self-excited cable motion are explained by the Den Hartog's quasi-steady treatment of the aerodynamic force with some modification.

1. INTRODUCTION

The cable system in which telecommunication line is suspended by steel aerial cable with lashing wires is widely used because the construction is relatively easy and cheap. This cable system has a particular geometric configuration of figure-8 as depicted in Fig. 1. It has been reported that wind-induced large amplitude galloping motion of cable of span 30 m or so frequently occurred under the wind with speed 10 to 20 m/s and caused serious operating problems, sometimes resulting in the failure of the cable system. Extensive studies on the galloping of ice-covered transmission cables or of bundled conductor cables have been made. However, since the figure-8 telecommunication cable cable were put into practice rather recently, our information on the galloping of this cable is far from complete and its detailed investigation is strongly needed.

The objectives of this study are to carefully observe the galloping phenomena of the telecommunication cables through the wind tunnel experiments employing three-dimensional scaled models and to offer an explanation for the fundamental cause of galloping of the figure-8 cable.

The experiments were conducted at the wind tunnels in the University of Tokyo and was confined to smooth flow.

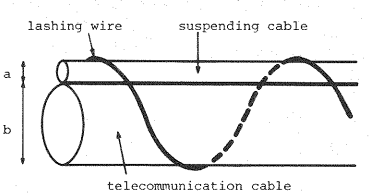

Fig. 1 Figure-8 telecommunication cable.

2. STEADY WIND FORCES

The steady wind forces, drag D, lift L and moment M on the

* Member of JSCE, Dr. Eng., Prof. of Civil Eng., Univ. of Tokyo (Bunkyo-ku, Tokyo)
** Member of JSCE, Ph. D, Assoc. Professor of Civil Eng., Univ. of Tokyo (Bunkyo-ku, Tokyo)
*** Member of JSCE, Dr. Eng., Asst. Professor of Foundation Eng., Saitama University (Urawa, Saitama)

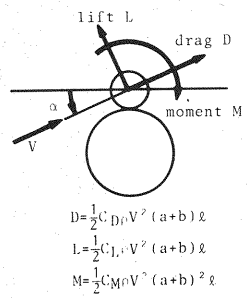

Fig. 2 Definition of steady wind force coefficients C_D, C_L and C_M.

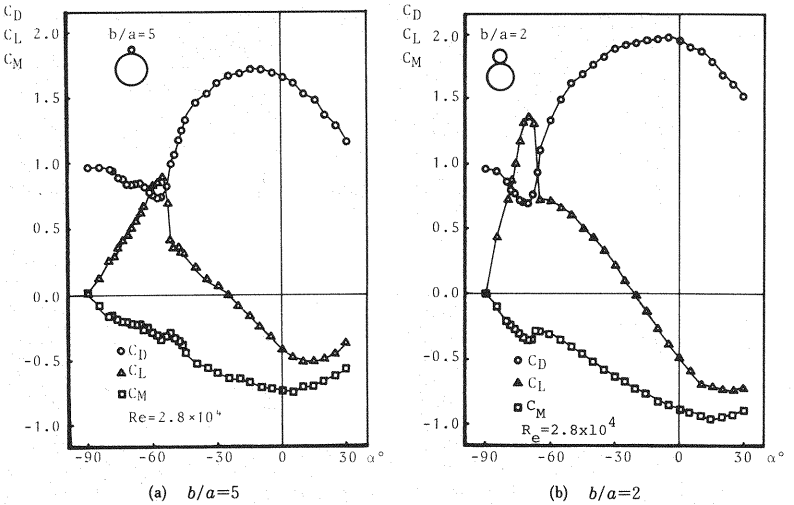

(a) $b/a=5$ (b) $b/a=2$

Fig. 3 C_D, C_L and C_M of figure-8 section vs. angle of wind attack, α.

figure-8 cable were experimentally measured using two-dimensional rigid models with end plates. Aluminum circular cylinders with smooth surface were used as the models. The diameter ratios b/a, in which a and b are the diameters of suspending cable and telecommunication one respectively, were selected as 2 and 5. Note that the ratio equal to 5 is the most typical value in the telecommunication lines. Since the cable section is figure-8, the effect of the Reynolds number was studied, but it was confirmed by the experiment that its effect on the steady wind forces is small over $R_e=10^4-10^5$. Fig. 2 shows the definition of force coefficients C_D, C_L and C_M while their values for a wide range of angle of wind attack, α are given in Fig. 3. It can be seen that large negative slope in both C_L-curves exists at the large negative angle of wind attack ($\alpha\doteqdot-55^\circ$ in $b/a=5$ and $\alpha\doteqdot-65^\circ$ in $b/a=2$), indicating the possibility of occurrence of galloping instability according to Den Hartog's explanation[1]. The wind tunnel experiment of the spring-supported two-dimensional model actually verified the galloping motion[2] for such a large angle of wind attack. The question arises whether the angle of wind attack due to a wind force reaches the unstable region or not. The experimental results in Fig. 3 indicate that overall characteristics of C_D, C_L and C_M in the two models are similar to each other. However, there is a small difference ; the angle corresponding to the drastic change in C_L-curve occurs at (negative) larger value of α for the smaller diameter ratio. According to the smoke wind tunnel experiments, this was found to be caused by the difference in the angles of wind attack at which the reattachment of the flow separated at the suspending cable occurs.

The wind force coefficients when lashing wire was attached to the cylinders were also experimentally measured and the effects of the lashing wire on the coefficients were found to be small.

3. WIND TUNNEL EXPERIMENTS OF FULL MODEL AND RESULTS

Two types of the full model were prepared and their model parameters are given in Table 1. In the models two vinyl tubes were lashed by very fine threads of which the diameter was 0.4 mm (Fig. 4). A piano wire was inserted into the smaller vinyl tube as a tensile member, while sand (Model I) or lead (Model II) was crammed into the larger tube in order to adjust the weight. The vinyl tubes readily available were used and therefore the diameter ratios in Models I and II are not exactly equal to 5 and 2, respectively. This figure-8 cable model of the span 15 m was suspended from two rigid frame supports in the wind tunnel of 16 m×1.9 m working section. The scale of this model is approximately 1/2. The experiments were conducted for various sag ratios. Static and dynamic displacements were measured by means of the targets of the electro optical displacement follower, attached to the cable models at quarter-

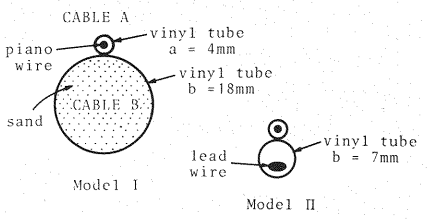

Fig. 4 Section of three-dimenstonal cable model.

Table 1 Model Parameters.

span		15 m	
suspending cable(cable A)	weight	25.0 g/m	
	diameter	4.0 mm	
	tensile rigidity, EA	3.31×10^5 kg m/s^2	
telecomm. cable(cable B)	weight	375.0 g/m (Model I)	61.9 g/m (Model II)
	diameter	18.0 mm (")	7.0 mm (")
logarithmic damping * (range)		0.02 - 0.05 (")	0.05 - 0.10 (")

* : first sym. and first asym. modes only, sag ratio 1%-5%(Model I),1%-3%(Model II)

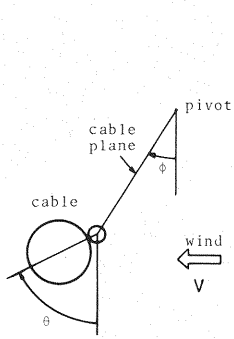

Fig. 5 Definition of angles, ϕ and θ.

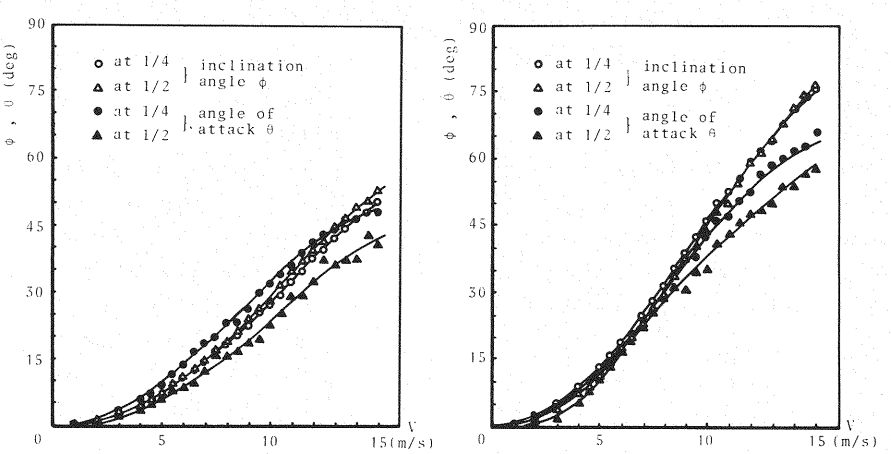

(a) Model I (b) Model II

Fig. 6 Static deformation angles ϕ and θ vs. wind speed V (sag ratio $r=0.03$).

and mid- spans.

(1) Wind-induced static deformation

Horizontal smooth wind flow transversely approaching the cable was employed. When the wind was turned on, the cable swung back to the wind force and reached an inclined static equilibrium position. This position was measured at different wind speeds which were increased in small steps. Fig. 5 shows the definition of the inclination angle of the cable (cable plane angle) ϕ as well as of the angle of attack of the cable relative to wind, $\theta(=-\alpha)$ and examples of their measured values are presented in Fig. 6. The angle of attack, θ as well as the cable inclination angle, ϕ increase monotonically as the wind speed increases. The inclination angles at quarter- and mid- spans are nearly equal to each other, indicating that the cable forms almost a plane even under a wind force.

On the other hand, the angle of attack, θ is apparently not uniform over the span ; the angle at quarter-span is larger than that at mid-span as shown in Fig. 6. One may attribute this fact to the yaw effect on the wind force to the cable ; the wind direction at quarter span is not normal to the axis of the cable. Quantitative effect of yaw on the wind forces in the figure-8 cable has not been investigated, and therefore we could not reach a definite answer to this. One can see in Fig. 6 that the angle of attack becomes larger for higher wind speeds and approaches the aerodynamically unstable region because large negative slope slope of C_L in large angle of attack $\theta(=-\alpha)$ exists as seen in Fig. 3.

For a given wind speed, the angle of attack, θ of Model II is larger than that of Model I which is heavier. Note that the weight of the target and chords for displacement measurement is approximately 45 g each point and is not negligible in comparison with that of Model II. The true angles ϕ and θ in Model II would be somewhat larger than those presented in Fig. 6 (b).

(2) Galloping motion

With further increase of the wind speed, the cable began to oscillate in a self-excited fashion. The vibration mode excited in Model I was mostly the first asymmetric one. Exceptionally, for the sag ratio is 0.02 and for the high wind speed (=15 m/s) the excited mode was not uniquely determined and was either first asymmetric, second symmetric or second asymmetric, depending upon the initial condition. The galloping mode in Model II was either the first asymmetric or the second asymmetric mode depending upon the sag and the wind speed. For the sag ratios from 0.01 to 0.03 in Model II, the second asymmetric mode appeared easily at the wind speed greater than 13 m/s.

The critical self-starting wind speed of Model I with the sag ratio of 0.03 was approximately 11.5 m/s. Since the model scale is about 1/2 this wind speed in the wind tunnel corresponds to $11.5\times1.4=16$ m/s in the prototype, which is consistent to the critical speed observed in the actual telecommunication lines.

Fig. 7 (a) shows a typical growth process of the galloping oscillation at the quarter span, while an example of time history of vertical and horizontal motions is given in Fig. 7 (b). For a small amplitude range the motion stays in nearly a plane and large rotational (torsional) motion is not clearly noticeable. However, after reaching a certain vertical amplitude the telecommunication line 'B' starts rotating around the suspending cable 'A' and presently the horizontal and vertical amplitudes increase rapidly (Fig. 7 (b)). After ten periods or so, the vertical and horizontal motions are stabilized in an elliptical or close-to-circle locus with large rotation of the cable 'B' relative to the cable 'A' as depicted in Fig. 7 (c). It should be mentioned that the locus of steady-state motion was not always a clear single loop and, in some cases, consisted of double loops. Fig. 8 shows a Lissajous of motion of Model I for the case of $r=0.03$ and $V=13.5$ m/s; during the experiment, it was observed that the out-of-plane swinging motion of the first symmetric mode was additionally excited to noticeable degree. This out-of-plane swinging motion may be attributed to the coupling effect of the nonlinear dynamics of in- and out- plane cable motions. In the experiments, there was not a single case that the galloping motion stays in a plane with a small oscillation amplitude, and always the stabilized galloping motion is rather large and followed rotational motion.

It is interesting to note that the initial direction of galloping is neither vertical nor the same as the angle

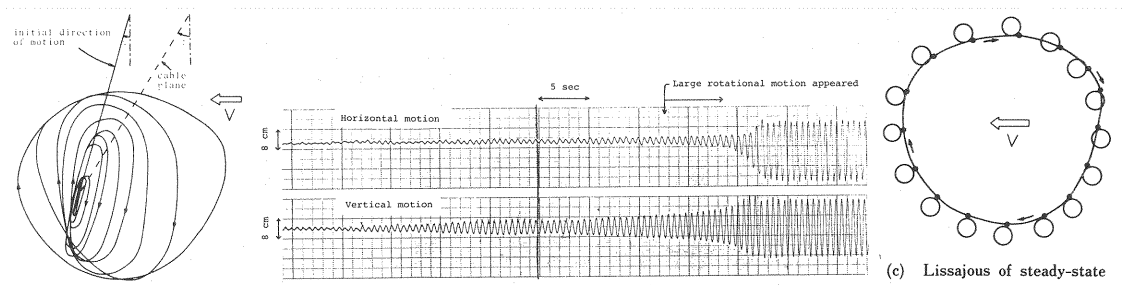

(a) Growth process ($V=11.5$ m/s). (b) Time-history of vertical and horizontal motions ($V=11.5$ m/s). (c) Lissajous of steady-state motion ($V=12$ m/s).

Fig. 7 Galloping motion in transverse plane at quarter span (Model I, sag ratio $r=0.03$).

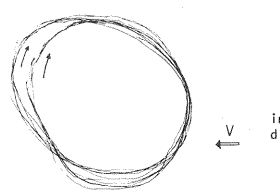

Fig. 8 Double loop Lissajous at quarter span (Model I, sag ratio $r=0.03$, $V=13.5$ m/s).

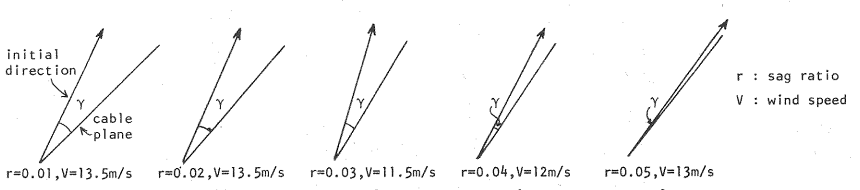

Fig. 9 Direction of initial motion for various sag ratios r at quarter span.

of inclination ϕ (Fig. 7 (a)). This angle was found to be smaller than ϕ as shown in Figs. 7 (a) and 9. A theoretical explanation regarding this initial direction is given afterwards.

The steady-state amplitudes of the first asymmetric mode at different wind speeds were also measured at quarter-span and are presented in Fig. 10 (a) (Model Ⅰ) and Fig. 10 (b) (Model Ⅱ). In these figures, nonstationary amplitude if exists is shown as a range. In Model Ⅰ as well as Model Ⅱ, the vertical and horizontal amplitudes of galloping increase for larger sag ratio. This can be explained by decrease of natural frequency when say is large. The amplitude measurements show that galloping of the fiqure-8 cable is a hard type and that the hysteresis characteristic is very weak. As seen in Fig. 3, large aerodynamic exciting force can be gained in the angle $\theta(=-\alpha)=55^\circ$ to 60° (Model Ⅰ) and $=60^\circ$ to 65° (Model Ⅱ). This aerodynamic property would cause the hard-type galloping.

As the wind speed increases, the amplitudes, especially the vertical amplitude does not increase noticeably and appears to be rather saturated, as seen in Fig. 10.

It should be mentioned that the angles of attack of the cable relative to wind, θ corresponding to the self-starting critical wind speed are smaller by 10° or so than the angle where sharp change of C_L values shown in Fig. 3.

It is well known that cable oscillation of the asymmetric in-plane modes possesses nonlinearity of a

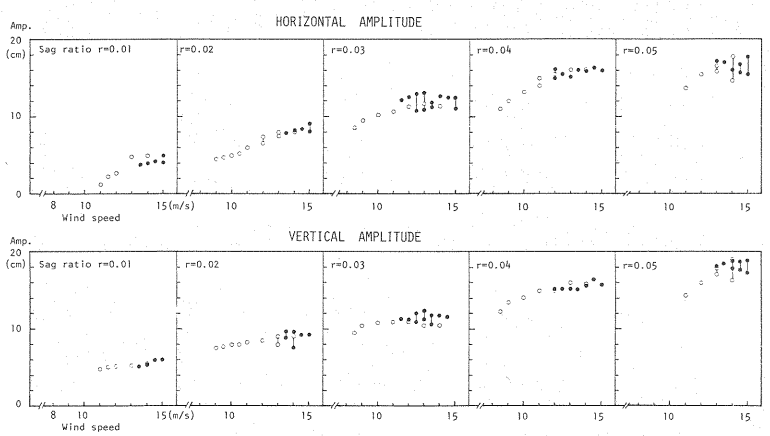

(a) Model Ⅰ

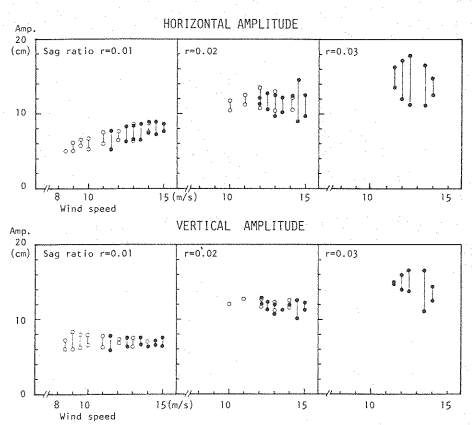

(b) Model Ⅱ

Fig. 10 Steady-state horizontal and vertical amplitudes of the first asymmetric mode at quarter-span (● : wind speed increased, ○ : wind speed decreased).

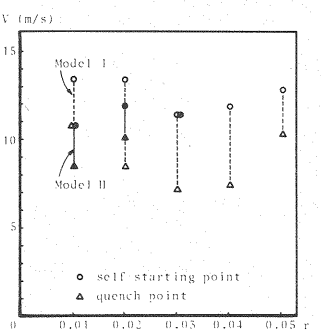

Fig. 11 Effect of sag ratio on critical galloping speed.

hardening type when its amplitude is large. However, since the amplitude of galloping motion is much less than the sag, this nonlinear effect would not contribute much to the saturation of the amplitude. Probably the large amount of rotational motion of the cable is more closely associated with the saturation phenomena.

The effect of the sag ratio r on the critical wind speeds is shown in Fig. 11. The experimental results presented in Fig. 11 show interstingly that, although the amplitude increases for larger sag ratio (Fig. 10 (a) and 10 (b)), the critical wind speed does not vary significantly for different values of sag ratio.

The galloping motion was also observed for the three-dimensional model of the diameter ratio b/a

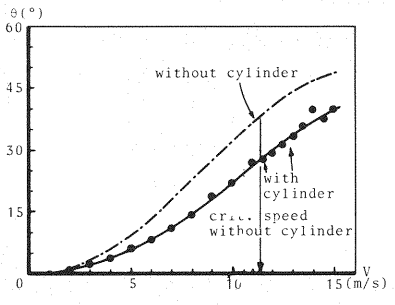

Fig. 12 Effect of 28 % cylinder coverage on static angle of attack θ (Model I, sag ratio $r=0.03$).

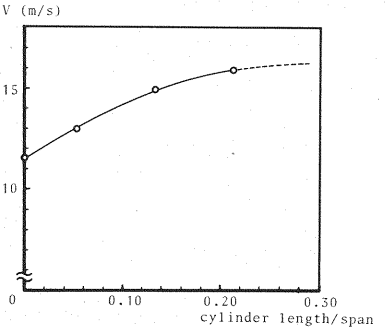

Fig. 13 Self-starting critical wind speed of the first asymmetric mode vs. cylinder length (Model I, sag ratio $r=0.03$).

equal to 1 but the results are not presented here. The self-starting wind speed was found to be around 9–13 m/s depending on the sag ratio of 0.01 to 0.03[2]. It can be said that for a wide range of the diameter ratio the figure-8 cable has inherent tendency to galloping instability even under not extremely high wind speed.

(3) Suppression of galloping motion

Finally, a control means of galloping was studied experimentally; cylinders of finite length were employed to cover the figure-8 cable. The cylinders are made of papers and very light. Therefore the mass of the cable is increased very little. Circular section is recognized to be aerodynamically stable against galloping. The cylinder of equal length were placed at the two quarter points of the Model I of the sag ratio 0.03. The angle of wind attack measured at quarter point when two cylinders covered 28 % (14 % each) of the span is presented in Fig. 12, where the angle of attack θ without the cylinders are also given for comparison. Fig. 12 shows large reduction of the angle due to the attachment of the cylinder. Employing cylinders as coverage thereby increases the tendency to stability of a figure-8 cable. The effect of the coverage on the critical self-starting wind speed of galloping of the first asymmetric is shown in Fig. 13; the abscissa is the ratio of coverage length to the cable span length, while the ordinate is the self-starting wind speed. Twenty percentage coverage increases critical speed by approximately 30 %, suggesting that this means is effective, at least for the asymmetric mode, to increase the stability.

4. DISCUSSIONS

Galloping is a self-excited oscillation due to the negative aerodynamic damping induced by the transverse motion of the body. This explanation is first given by Den Hartog[1]. The galloping oscillation of power transmission cables or rectangular bodies has been studied extensively by many researchers, including Parkinson[3] and Novak[4]. The general agreement between theory and experiment has proved the effectiveness of using a quasi-steady approach. The reduced velocity of galloping in Model I and Model II is well above 100 for vertical (horizontal) motion and even for rotational motion. Applicability of the quasi-steady approach is therefore believed to be quite reasonable. First, consider the fundamental cause of the galloping of a figure-8 suspended cable. Rotational motion is not taken into account in the following consideration since the experimental observation shows the rotational motion is small in the initial stage of galloping, i.e., for a small vertical amplitude.

Suppose that the cable moves to the direction ψ from vertical with the velocity $\dot{\eta}$ as shown in Fig. 14. Then, the net aerodynamic force F_η per unit length is given by the quasi-steady theory as

$$F_\eta=\frac{1}{2}\rho(a+b)V^2C_{F\eta} \quad \cdots\cdots (1)$$

where ρ=air density, $a+b$=width of the cross section (see Fig. 2), V=wind speed, and $C_{F\eta}$=

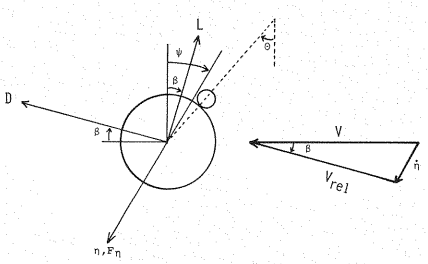

Fig. 14 Aerodynamic force on cable.

aerodynamic force coefficient. Using the wind force coefficients C_D and C_L given in Fig. 3, the aerodynamic force coefficient $C_{F\eta}$ can be expressed as

$$C_{F\eta}=\left(\frac{V_{rel}}{V}\right)^2[C_D(\alpha)\sin(\psi-\beta) - C_L(\alpha)\cos(\psi-\beta)] \quad \cdots\cdots (2)$$

in which the relative wind speed V_{rel} and the angle of wind attack β are defined in Fig. 14. The following relation can be easily obtained

$$\left(\frac{V_{rel}}{V}\right)^2=\frac{\cos^2\psi}{\cos^2(\psi-\beta)} \quad \cdots\cdots (3)$$

From Eqs. (2) and (3), the aerodynamic condition for the onset of soft galloping is given as

$$A_1=\left(\frac{dC_{F\eta}}{d\alpha}\right)_{\alpha=-\theta}=\frac{1}{\cos\psi}\left[\left(C_D-\frac{dC_L}{d\alpha}\right)\cos^2\psi-2C_D+\left(\frac{dC_D}{d\alpha}+C_L\right)\sin\psi\cos\psi\right]_{\alpha=-\theta}>0 \quad \cdots\cdots (4)$$

Eq. 4 is a generalization of the well known Den Hartog's condition given by

$$A_1=-\left(C_D+\frac{dC_L}{d\alpha}\right)_{\alpha=-\theta}>0 \quad \cdots\cdots (5)$$

Note that Eq. 4 is identical to Eq. 5 when $\psi=0$. When the body oscillates not transversely to the wind direction, the galloping condition is determined by not only C_D and $dC_L/d\alpha$, but also $dC_D/d\alpha$, C_L and the angle ψ, as seen in Eq. 4. At $\theta=45^\circ$ to $55^\circ(=-\alpha)$ of Model I, C_D drastically decreases, consequently $dC_D/d\alpha>0$. Furthermore C_L is positive as shown in Fig. 3 (a); A_1 in Eq. 4 could be positive under these condition. Similarly, A_1 of the Model II could be positive at $\theta=55^\circ$ to 60° (Fig. 3 (b)).

The value of A_1 for Model I was calculated using the 7-th order polynomial approximation of the coefficients C_D and C_L presented in Fig. 3 (a) and the results at the wind speeds 11.5 m/s and 12.5 m/s for the case of the sag ratio 0.03 are shown in Fig. 15. The diameter ratio in Model I is $b/a=4.5$, whereas C_D and C_L values are from the figure-8 section of $b/a=5$. Therefore, calculated value of A_1 should not be considered to be exact. Value of the angle θ is taken from the static measurement shown in Fig. 6 (a). A few comments should be stated regarding Fig. 15. At the wind speed 11.5 m/s corresponding to the self-starting speed in the experiment, the value of A_1 is negative for any direction of ψ, but at the speed 12.5 m/s the value of A_1 is changed into positive values for a certain region of ψ, indicating that galloping of the self-starting type may occur. In Fig. 15 (b) the maximum of A_1 i. e. largest exciting force occure at

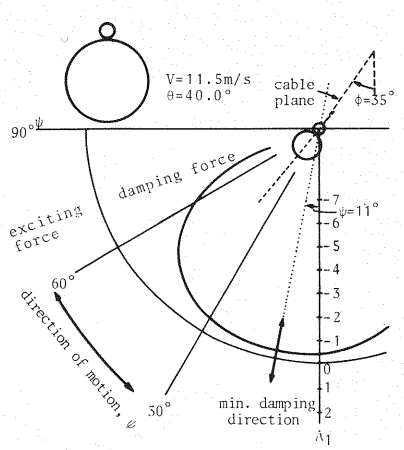

(a) $V=11.5$ m/s, $\theta=40^\circ$

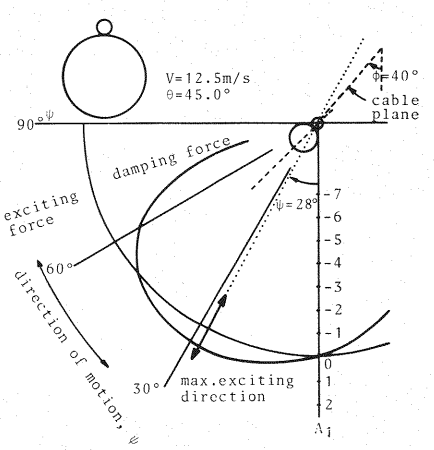

(b) $V=12.5$ m/s, $\theta=45^\circ$

Fig. 15 Velocity proportional coefficient A_1 vs. direction of cable motion ψ (Model I, sag ratio $r=0.03$).

$\psi=28^\circ$, neither at $\psi=0^\circ$ (vertical direction) not at 40° (cable plane angle). This angle $\psi=28^\circ$ is smaller than the cable plane angle 40° (measured) and is close to the measured angle of the self-excited motion in a small amplitude range. Since the cable is equally flexible to any direction in the asymmetric modes, it is not unnatural that the initial direction of instability motion coincides with the direction of the largest aerodynamic exciting force.

Secondly we would like to discuss the results shown in Fig. 11. As well known, the critical self-starting wind speed of galloping under a given configuration of the bluff body, is determined by the structural natural frequency and damping. In the case of an aerial figure-8 flexible cable, however, it should be born in mind that the static angle of wind attack θ is a function of the wind speed as shown in Fig. 6. According to our calculation, $A_{1\max}$ in Model I was positive only for θ greater than 43° and increases significantly as the angle of wind attack increase up to 54°[5]. The wind speed corresponding to the angle $\theta=43^\circ$ at quarter span can be read from Fig. 16 : approximately $V=15$ m/s (sag ratio $r=0.01$), 12—13 m/s ($r=0.02$ to 0.05). These critical wind speeds are not completely, but qualitatively coincident with the experimental data in Fig. 11. Conclusively, the critical wind speed is determined principally by the wind-induced static angle of attack of the cable relative to wind, θ and meanwhile the natural frequency and the structural damping seemingly give seconday influence on it. This is the most characteristic feature of galloping of the aerial figure-8 cables. Regarding Model II, the instability ($A_{1\max}>0$) occurs at larger $\theta(>43^\circ)$ as aforementioned but one can notice in Fig. 6 that the speed static angle of attack θ in Model II is larger than that θ of Model I, consequently leading to the critical self-starting wind speeds more or less equal to those in Model I. So far, the fundamental cause of galloping is investigated as a single-degree-of-freedom oscillator. As mentioned, however, detail observation of galloping motion indicates that rotational motion (θ-direction) is seemingly coupled to some degree with the vertical motion of cable even for a small amplitude range. This coupling may be a structural or aerodynamic one. Further careful observation of the experiment is certainly needed and the effect of the coupling motion on the galloping, especially on the self-starting critical velocity will have to be studied.

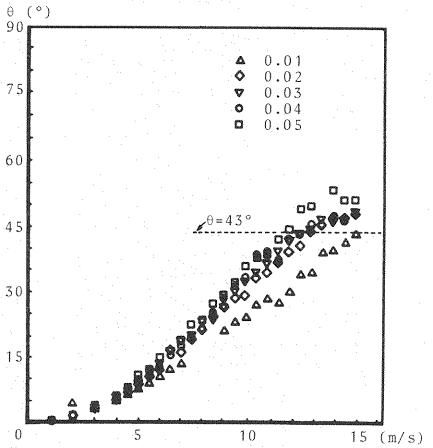

Fig. 16 Static angle of wind attack for sag ratios 0.01 to 0.05 (Model I).

Oscillation mode of the galloping of cable should be another interesting topic. As previously mentioned, the excited modes in the experiments were practically asymmetric ones and the first symmetric mode never appeared. However, it should be noted that the first symmetric mode was excited at the Model I in the preliminary experiment where rather flexible supports were employed. Since the vibration of the supports induced by the galloping motion of the cable, was so violent, the supports were reinforced and since then the first symmetric mode had not been excited in the galloping. It is reported that the observed galloping mode of the actual figure-8 telecommunication cables is mostly first asymmetric but, in some cases, first symmetric. Flexibility of cable supports is an important factor to account for the principal oscillation mode of the cable galloping.

5. CONCLUDING RFMARKS

Wind tunnel testing of the figure-8 telecommunication aerial cable using full model was conducted under smooth flow and its aeroelastic behaviour was studied. Theoretical considerations were also made on the fundamental cause of the galloping of the figure-8 suspended cable. Results of this study lead to the following brief conclusions :

(1) It is found that galloping of the figure-8 telecommunication cable can be well simulated using the

three dimensional model in the wind tunnel.

(2) An interesting phenomenon was observed in the course of the growth galloping. In a small amplitude range, the oscillation stays nearly in a plane and its direction is between the vertical and the cable plane inclined owing to the wind force. After reaching a certain amplitude, the rotational motion appears and the amplitude increases considerably in horizontal as well as vertical directions, resulting finally in an elliptical or close-to-circle steady-state motion with significant amount or rotational motion.

(3) As the sag ratio increases, the amplitude of the galloping increases, but the critical wind speed stays rather constant. It is also found that the critical wind speed is not so sensitive to diameter ratio of figure-8 cable, natural frequency, damping and sag ratio. The saturation of the amplitude, especially of the vertical one for higher wind speeds are observed in the experiments.

(4) The aerodynamic condition for the onset of soft galloping when the motion is not transverse to the wind flow is derived ; this is a generalization of Den Hartog's condition. This condition explains the critical self-starting wind speed of the galloping and furthermore the galloping direction in a small amplitude range. The fundamental cause of the galloping is found to be the change of the wind attack angle, due to the aerodynamic steady force.

In this study, theoretical prediction of the galloping of figure-8 cables employing a continuous cable model is not explored. An attempt to this problem is reported in Ref. 7.

6. ACKNOWLEDGMENTS

Financial support by the Tsukuba Construction Engineering Office, Nippon Telegram and Telephone and the Ministry of Education, Science and Culture, Japan under Grant-in-Aid for Scientific Research is gratefully acknowledged. Thanks are also due to I. Tsuruta, K. Momura, K. Oguri, K. Ohtake, M. Ikeda, and H. Fukazawa for their assistance in the wind tunnel experiments.

REFERENCES

1) Den Hartog, J. P. : *Mechanical Vibration*, McGraw-Hill, 1934.
2) Tsuruta, I. : Areoelastic Instability Oscillations of Suspended Figure-8 Telecommunication Cables, Master's Thesis, Dept. of Civil Eng., Univ. of Tokyo, 1983 (in Japanese).
3) Parkinson, G. B. and Smith, J. D. : The Square Prism as Aeroelastic Non-linear Oscillator, Quart. Journal of Mech. and Appl. Math., Vol. XVII, pt. 2, Oxford Univ. Press, pp. 225～239, 1964.
4) Novak, M. and Tanaka, H. : Effect of Turbulence on Galloping Instability, Proc. ASCE, Journal of the Eng. Mech. Division, Vol. 100, No. EM 1, pp. 27～47, 1974.
5) Fukazawa, H. : Aeroelastic Behavior of Suspended Telecommunication Cables, Graduation Thesis, Dept. of Foundation Eng., Saitama Univ., 1984 (in Japanese).
6) Nomura, K. : Experimental and Analytical Study on Wind-excited Oscillations of Figure-8 Suspended Cables, Graduation Thesis, Dept. of Civil Eng., Univ. of Tokyo, 1984 (in Japanese).
7) Yamaguchi, H., Yamawaki, Y., Fujino, Y. and Ito, M. : Analytical Study of an Overhead Figure-8 Telecommunication Line under a Steady Wind, Proc. of JSCE, Struct. Eng./Earthq. Eng., Vol. 2, No. 1, pp. 235 s～244 s, 1985.

(Received August 17 1984)